DSP Control of Current Sourcing Inverters

Ilya Zeltser and Professor Sam Ben-Yaakov
Power Electronics Laboratory
Department of Electrical and Computer Engineering
Ben-Gurion University of the Negev
P.O. Box 653, Beer-Sheva 84105, ISRAEL.
Phone: +972-8-646-1556; +972-54-6657754; Fax: +972-8-647-2949;

Emails: ilyaz@ee.bgu.ac.il, sby@ee.bgu.ac.il; Website: www.ee.bgu.ac.il/~pel

Abstract

Grid connected inverters are important building blocks in renewable energy conversion systems. In conventional voltage sourcing grid connected inverters, any mismatch between the synthesized output waveforms of the inverters and the grid voltage will generate large erroneous currents unless a fast current feedback is used. The current control requires rather fast sampling rates and considerable DSP resources as well as independent hardware for protection. An alternative approach to the voltage sourcing design is to apply an inverter with an Output Current Sourcing (OCS) behaviour. Current sourcing at the output implies that, ideally, the injected current will be independent on the load voltage. This study describes a DSP control of a soft switched OCS grid connected inverter that applies a high frequency isolation transformer and does not include a costly resonant capacitor. All the required control and housekeeping functions are implemented on a TMS320F2808 DSP core of Texas Instruments.

The proposed topology and possible control approaches were tested on a 3.5kW prototype. The experimental results show that the proposed DSP controlled inverter acts as a stable current source and attests to the powerful capabilities of the TI TMS320F2808 in switch mode power conversion systems.

1. Introduction

Grid connected inverters are important building blocks in renewable energy conversion systems [1-10]. In conventional voltage sourcing grid connected inverters, any mismatch between the synthesized output waveforms of the inverters and the grid voltage will generate large erroneous currents unless a fast current feedback is used. The current control requires rather fast sampling rates and considerable DSP resources as well as independent hardware for protection. An alternative approach to the voltage sourcing design is to apply an inverter with an Output Current Sourcing (OCS) behavior. Current sourcing at the output implies that, ideally, the injected current will be independent on the load voltage. Consequently the current feedback loop can be omitted, shortening significantly the DSP computation time, reducing the number of the required sampling circuits and eliminating extra protection hardware and thereby reducing the component count of the system.

Grid connected OCS inverters were presented in [11] applying a flyback converter while in [12] it was based on a series resonant converter followed by a diode rectifier and a polarity commutator. To exhibit the OCS characteristics the circuit in [12] must be operated below half the resonant frequency (discontinuous current conduction mode) and consequently, the reactive current in the resonant tank is expected to be high, especially at high power levels, and the resonant capacitor will have large physical dimensions.

This study describes a DSP control of a soft switched OCS grid connected inverter that applies a high frequency isolation transformer and does not include a costly resonant

capacitor. The current injected to the line is controlled by varying the switching frequency. All the required control and housekeeping functions are implemented on TMS320F2808 DSP core of Texas Instruments.

2. System Description

The topology of the proposed inverter is based on the "AC inductor" concept described in [13]. “AC inductors” have several advantages over “DC inductors” [13]: (1) the current in “AC inductors” reverses its polarity every switching cycle making it easier to achieve soft switching; (2) the average low frequency component of the voltage across the “AC inductors” remains zero reducing significantly the risk of a current run away; and importantly, (3) “AC inductors” exhibit an OCS behavior and hence they are less sensitive to the output voltage waveform shape and distortion and to disturbances at either input or load side.

The proposed inverter comprises two H bridges Q_1-Q_4 and Q_5-Q_8 (Fig. 1), a main inductor L_{in}, high frequency isolating transformer T1 and output rectifier D_1-D_4. The input bridge, which operates under zero voltage switching conditions at turn on, generates a high frequency symmetrical square wave that is applied to the main inductor. The triangular current of the inductor is reflected to the secondary of the isolating transformer T1 and rectified by D_1-D_4. The rectified current is filtered by the output filter (C_F, L_F in Fig. 1) and fed to the line through the output bridge Q_5-Q_8 that is synchronized to the line and acts as a polarity commutator.

Since the switching frequency of the input bridge is much higher than the line cycle, one can assume that the voltage V_{out} applied to the output rectifier at every given time instant (t) of the line cycle is practically constant. Consequently, the high frequency portion of the inverter can be analyzed by considering that the output voltage is constant as was described in [13]. For the sake of brevity only essentials are repeated here.

During the time interval t_1-t_2 (Fig. 2) of the high frequency switching cycle, the peak inductor current Ipk is:

$$Ipk = \frac{V_{bus} - V_{out}}{L_{in}}(t_2 - t_1) \tag{1}$$

where L is the inductance of the inductor. Similarly, during the time interval t2-t3 Ipk is expressed as:

$$Ipk = \frac{V_{bus} + V_{out}}{L_{in}}(t_3 - t_2) \tag{2}$$

From (1) and (2), taking into account that (t_3-t_1) is half a switching cycle, yields:

$$(t_2 - t_1) + (t_3 - t_2) = I_{pk} L_{in} \frac{2V_{bus}}{V_{bus}^2 - V_{out}^2} = \frac{1}{2F} \tag{3}$$

where F is the switching frequency.

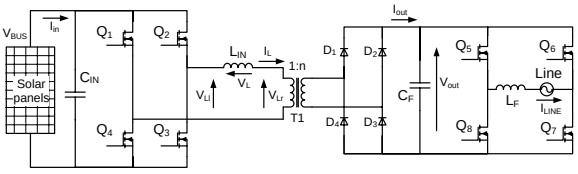

Figure 1: Power stage of the proposed grid connected inverter

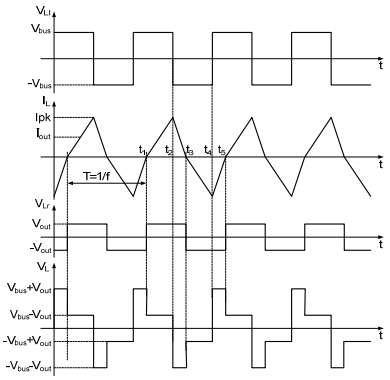

Figure 2: Basic waveforms of the proposed inverter, for n=1.
From top to bottom: V_{L1}, Inductor current I_L, V_{Lr}, voltage across inductor

Rearranging (3) back for Ipk we get:

$$Ipk = \frac{V_{bus}^2 - V_{out}^2}{4L_{in}FV_{bus}} \tag{4}$$

The output current is the rectified inductor's current as depicted in Fig. 3. Since the output current is of triangular shape, its average value is half its peak value:

$$\bar{I}_{out} = \frac{1}{2}Ipk = \frac{V_{bus}^2 - V_{out}^2}{8L_{in}FV_{bus}} \tag{5}$$

where $\bar{I}_{out}$ is the output current averaged over the switching cycle.

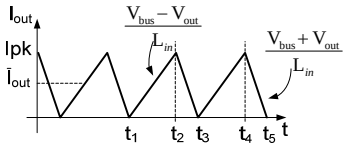

Figure 3: Zoom on I_{out} (Fig. 1).

During the line cycle the output voltage V_{out} will follow the line voltage, i.e. $V_{out}=V_{line}(t)$:
It is assumed that the line voltage is of form:

$$V_{line}(t) = V_{rms}\sqrt{2}\sin 2\pi f_{line}t \tag{6}$$

where V_{rms} is rms line voltage, f_{line}- line frequency.
Considering (6), (5) can be rewritten as follows:

$$\bar{I}_{out}(t) = \frac{V_{bus}^2 - V_{line}^2(t)}{8 \cdot L_{in} \cdot F(t)V_{bus}} \tag{7}$$

where $\bar{I}_{out}(t)$ is the average output current of the inverter and F(t) is the switching frequency at time instant t.

Since the goal of a grid connected inverter is to deliver a current which is in phase with and of the shape of the line voltage, the inverters output current should be of the form:

$$\bar{I}_{out}(t) = I_{rms}\sqrt{2}\sin 2\pi f_{line}t = \frac{P_{out}}{V_{rms}}\sqrt{2}\sin 2\pi f_{line}t \tag{8}$$

Where I_{rms} is rms line current, P_{out} – average power delivered to the line.

Considering (6), (8) can be rewritten as follows:

$$\bar{I}_{out}(t) = \frac{P_{out} V_{line}(t)}{V_{rms}^2} \tag{9}$$

From (9) and (7) we get:

$$F(t) = K_p \frac{V_{bus}^2 - V_{line}^2(t)}{V_{line}(t)}, \text{ where } K_p = \frac{V_{rms}^2}{8 L_{in} P_{out} V_{bus}} \tag{10}$$

Based on (10), three different control approaches can be considered. One option is to measure the instantaneous line voltage $V_{line}(t)$ by sampling, for example, the line using the internal A/D converter of the DSP. The program run on DSP will then apply the sampled value to calculate the required frequency F(t) of the input bridge gate pulses according to (10). The coefficient K_p can be considered as a scaling factor that will be obtained from the Maximum Power Point Tracking (MPPT) algorithm such that, for any given operating conditions, K_p will be adjusted as required to obtain the maximum power available from the photovoltaic cell panels.

Another option for deriving F(t) is for DSP to measure only the rms value of the line voltage (much lower sampling rate) and calculate the V_{line} according to (2). For this case, (10) can be rewritten as follows:

$$F(t) = K_p \frac{V_{bus}^2 - 2V_{rms}^2 \sin(2\pi f_{line} t)}{V_{rms} \sin(2\pi f_{line} t)} \tag{11}$$

Yet another control option would be to calculate the frequency without sensing the line voltage at all. The drive frequency F(t) will be calculated by the DSP in this case by assuming some predefined (nominal) rms value of the line voltage (V_{nom}):

$$F(t) = K_p \frac{V_{bus}^2 - 2V_{nom}^2 \sin(2\pi f_{line} t)}{V_{nom} \sin(2\pi f_{line} t)} \tag{12}$$

Although there is no need to measure the line voltage in this case, there would be a need to synchronize the operation to the line frequency by, for example, sensing the zero crossing of the line voltage.

It should be stressed though that none of the above mentioned control methods require the sensing of the output current.

From the practical point of view, the first approach is the most complicated one as it requires line sensing circuitry with rather high sampling rate. In the second case, the sampling rate can be much lower as only the rms value of the line voltage needs to be measured. However, the current injected to the line may be slightly distorted. The third method is the simplest among the suggested control approaches since no sensing circuitry is needed. On the other hand, the THD of the current generated in this case will increase as the difference between the nominal and actual rms values of the line voltage increases.

In all three alternatives (10-12) the frequency needs to go to high (and even impractical) values around the zero crossing of the line voltage when the magnitude of the injected current needs to be small. One possible approach to overcome this practical limitation is to limit the drive frequency to some maximum value F_{lim} and to apply dithering, that is, periods of global 'on' and 'off' sequences of the drive at a lower modulating frequency.

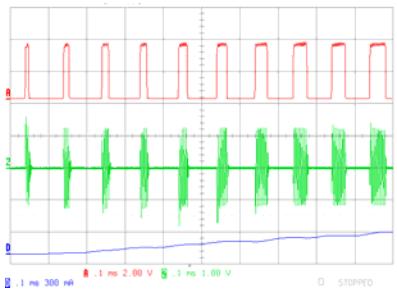

Figure 4: Dithering mode around zero cross.
Upper trace: modulating carrier; middle trace: inductor's current;
lower trace: filtered output current.

Namely, to skip switching cycles so as to obtain the required average value of the output current. The required global duty cycle will thus be:

$$D_G(t) = \frac{F_{\lim}}{F(t)} \tag{13}$$

where F(t) is the frequency calculated according to (10-12).

The effect of the switching cycle skipping on the output current is demonstrated in Fig. 4.

3. System control and DSP Utilization

The experimental control circuitry of the proposed OCS grid connected inverter includes a DSP evaluation board (Fig. 5), input and output sensing circuits, synchronization unit and floating drivers.

The control circuitry is governed by the control algorithm that is implemented in C. The code was designed using Code Composer Studio 3.1.23 from TI.

Upon systems power on the control algorithm initializes the peripheral units (i.e. PWM, GPIO, timer and A/D) and defines the run time variables (Blocks 1&2 in Fig. 6a). Then the frequency and duty cycle values for the entire line cycle are calculated according to (12) and saved in the appropriate tables (block 3). These values are used to generate the pulses that drive the input H bridge (Q1-Q4).

After sampling the input and output voltages the algorithm verifies that the output of the PV panels is high enough to start the normal operation (block 5 in Fig. 6). Then, the soft start procedure (block 6) is initiated. During the soft start, the output bridge (Q5-Q8) is enabled, the duty cycle of the input bridge is increased gradually from 0 to 50% and the system is moved to a normal operation mode.

While in the normal operation (Fig. 6b), the input H bridge (Q1-Q4) is driven by variable frequency bipolar square wave signal with 50% duty cycle. The frequency (F(t)) is varied

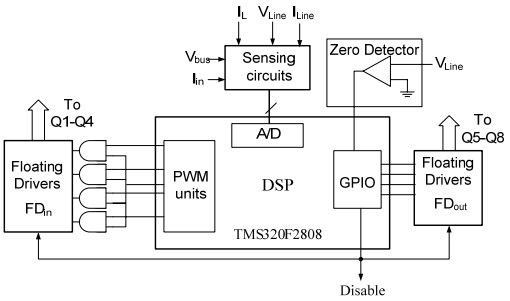

Figure 5: DSP based control circuit of the proposed OCS inverter

during the line cycle according to (10-12) to obtain a sinusoidal output current. The values for the F(t) is taken from the tables prepared in the block 3 of the control algorithm. These values are used as are if the control approach with no sensing of the line voltage is chosen. In case of sensing the output voltage the values stored in the tables are first modified according to the measured instantaneous line voltage (eq. 11) or according to the measured rms value of the line voltage (eq. 10) The gate pulses to the input H-bridge are generated using PWM units of TMS320F2808 (Fig. 5) that are synchronized to each other. The gating pulses are provided to the gates via four floating drivers FD_{in} (Fig. 5). One extra PWM unit is used to generate a low frequency modulating carrier (upper trace in Fig. 4). This signal is multiplied (logical "AND") with the outputs of the other PWMs (Fig. 5). The frequency of this carrier is constant and was chosen to be above the audio frequencies range but below the minimal switching frequency of the input bridge. The duty cycle of this signal is programmed according to (13). When the skipping is not necessary its duty cycle is set to unity.

If one of the measured parameters is beyond its normal operating range, both FD_{in} and FD_{out} are disabled by activating the output "Disable" (Fig. 5) Then the protection algorithm is initiated (block 10) and the control algorithm returns to the start up sequence (entry A in Fig. 6a).

The line synchronization signal is provided to DSP by an external zero crossing detector. The output of this detector is logic "1" when the line is positive and it is logic "0" when the line is negative. This signal is connected to one of the GPIO ports and "translated" to the gate signals of the switches Q5-Q8 via the floating drivers FD_{out}. If the synchronization signal is at its high state (line is positive) the control algorithm sets the gates of Q5 and Q8 to "1" and those of Q6 and Q7 to "0". When the synchronization signal is zero (line is negative) Q6 and Q7 will conduct and Q5 and Q8 will not. The synchronization signal is checked at constant sampling rate defined by the internal timer. When the predefined time interval terminates the timer initiates the interrupt routine described in Fig. 6c. Apart from checking the status of the zero detector and updating the pulses to the output bridge the routine updates the time variable that indicates the time t elapsed from the beginning of the line cycle (block 13). This variable is used by "normal operation" routine (control block 11) to "pick up" the frequency that corresponds to the time instant t.

Another timer will be used to start the MPPT algorithm (not shown and/or implemented in this study) that will multiply the values stored in the frequency table by the constant K_p (10-12) according to the measured V_{bus} and I_{in}. This will adjust the inductor's current to correspond to the power available from the power cells.

The input and output voltages and currents were measured by dedicated external sensing circuits and sampled by internal A/D's of TMS320F2808.

It should be noticed that not all the functions described above were yet implemented.

4. Experimental

All the three proposed control methodologies were verified by a cycle-by-cycle simulations as well as by a behavioral simulation model of the proposed current sourcing inverter. Good agreement was found between the theoretical predictions and the simulation.

The behavior of the proposed "AC inductor" based OCS inverter was tested experimentally on a 3.5kW prototype that was based on the topology shown in Fig. 1 and was powered by a DC voltage source. The value of the main inductor was 28μH. The switching frequency varied from 30kHz at the middle of the line cycle up to 200kHz. Near the zero crossings of the line voltage the switching cycles of the input bridge were dithered 30kHz to obtain

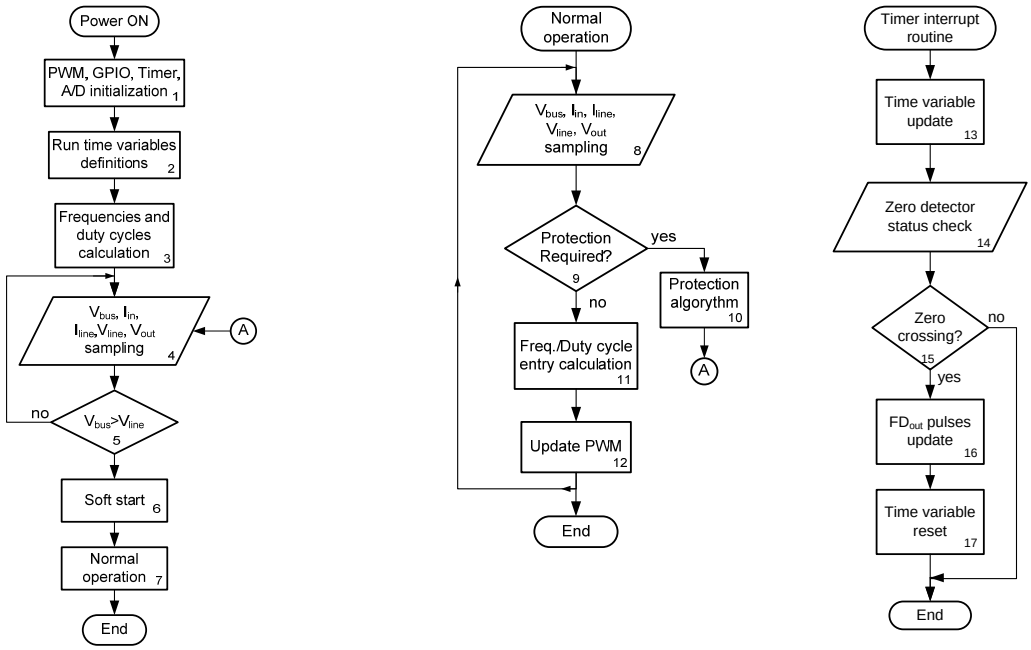

Figure 6: Block diagram of control algorithm.
(a) Start-up sequence, (b) Normal operation, (c) Timer interrupt routine

sinusoidal shaped average current while staying at the constant switching frequency of 200kHz. The circuit was controlled by a DSP (TMS320F2808, TI). Tests were run up to 1kW.

Fig. 7 shows the output current measured when the inverter's output voltage was set to 110Vrms. Fig. 8 presents the current obtained for the case when the output of the inverter was shorted. In both cases the switching frequency was generated according to (10) assuming a V_{nom} value of 110V.

5. Discussions and Conclusions

This study presents an OCS soft switching inverter that is fully controlled by a DSP unit. The output current is generated by varying the switching frequency. All the control signals as well as the housekeeping functions are implemented using the DSP. All the switches are switched under zero voltage at turn on.

The simulation and experimental results show that the proposed inverter can be operated in open loop, i.e. with no need to sense the line current and even without sensing the line voltage – except for synchronization. This is in contrast to the conventional voltage sourcing inverters where a tight current feedback loop must be applied.

The current shape obtained in the control method with no sensing of the line voltage might get slightly distorted if the difference between the actual and assumed nominal rms values of

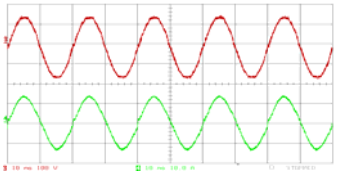

Figure 7: Output behavior of the inverter with no sensing of the output voltage.
Vin=318V; V_{line}=110Vrms; Pout=1kW.
Upper trace: output voltage 100V/div; Lower trace: line current (I_{LINE}) 10A/div; Horizontal scale: 10ms/div.

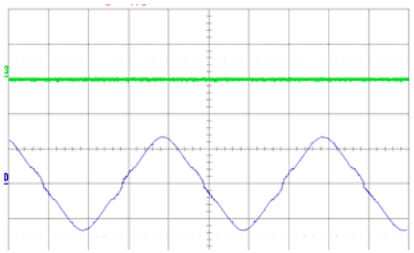

Figure 8: Output current of the inverter with shorted output. Vin=265V;
Upper trace: output voltage (shorted); Lower trace: line current (I_{LINE}) 10A/div; Horizontal scale: 5ms/div.

the line voltage is significant. However, due to the OCS capabilities of the proposed inverter, the generated output current was very close to the nominal sinusoid shape even when the output was shorted (Fig. 8).

The experimental results show that the proposed DSP controlled inverter acts as a stable current source and attests to the powerful capabilities of the TI TMS320F2808 in switch mode power conversion systems.

References

[1] F. Huang, G. Zhimin, T. Forughian, and D. Tien, "A new microcontroller based solar energy conversion modular unit," Power Conversion Conference - Nagaoka 1997., vol. 2, pp. 697-700, 3-6 Aug. 1997.

[2] K. Chomsuwan, P. Prisuwanna, and V. Monyakul, "Photovoltaic grid-connected inverter using two-switch buck-boost converter," Twenty-Ninth IEEE Photovoltaic Specialists Conference, 2002, pp. 1527 – 1530, 19-24 May 2002.

[3] Z. Chunjiang, C. Lingling, G. Herong, Z. Yanping, and W. Weiyang "Grid-connected inverters interface control with unified constant-frequency integration control," Eighth International Conference on Electrical Machines and Systems, ICEMS 2005, vol. 2, pp. 982–985, 27-29 Sept. 2005.

[4] Y. Chen and K. M. Smedley, "A cost-effective single-stage inverter with maximum power point tracking," IEEE Transactions on Power Electronics, issue 5, vol. 19, pp. 1289-1294, Sept. 2004.

[5] K. Hirachi, M. Ishitobi, K. Matsumoto, H. Hattori, M. Ishibashi, M. Nakaoka, N. Takahashi, and Y. Kato, "Pulse area modulation control implementation for single-phase current source-fed inverter for solar photovoltaic power conditioner," 1998 International Conference on Power Electronic Drives and Energy Systems for Industrial Growth 1998, vol. 2, pp. 677-682, 1-3 Dec. 1998.

[6] Mihai Ciobotaru, Remus Teodorescu and Frede Blaabjerg, "Control of single-stage single-phase PV inverter," *European Conference on Power Electronics and Applications 2005, pp. 1-10, 11-14 Sept. 2005.*

[7] D. C. Martins and R. Demonti, "Interconnection of a photovoltaic panels array to a single-phase utility line from a static conversion system," IEEE 31st Annual Power Electronics Specialists Conference, PESC 00, vol 3, pp. 1207 – 1211, 18-23 June 2000.

[8] T. Takebayashi, H. Nakata, M. Eguchi, and H. Kodama, "New current feedback control method for solar energy inverter using digital signal processor," Power Conversion Conference - Nagaoka 1997, vol. 2, pp. 687–690, 3-6 Aug. 1997.

[9] S. Saha, N. Matsui, and V. P. Sundarsingh, "Design of a low power utility interactive photovoltaic inverter," 1998 International Conference on Power Electronic Drives and Energy Systems for Industrial Growth, 1998, vol 1, pp. 481–487, 1-3 Dec. 1998.

[10] D. A. Torrey, S. Kittiratsatcha, T. B. Bashaw, and R. T. Carpenter, "Inverter topology for utility-interactive distributed generation sources," U. S. Patent 2005/0180175 A1, August 18, 2005.

[11] A. C. Kyritsis, N. P. Papanikolaou, E. C. Tatakis, and J. C. Kobougias, "Design and control of a current source flyback inverter for decentralized grid connected photovoltaic systems," European Conference on Power Electronics and Applications, 2005, pp. 1-10, 11-14 Sept. 2005.

[12] K. Al-Haddad, R. Chaffai, and Rajagopalan, "High frequency inverter using zero current turn off COMFET switches for solar energy conversion," 12th International Telecommunications Energy Conference, INTELEC '90, pp. 41-46, 21-25 Oct. 1990.

[13] I. Zeltser and S. Ben-Yaakov, "Modeling, analysis and simulation of "AC inductor" based converters," Power Electronics Specialists Conference 2007, PESC 2007, pp. 2128 – 2134, 17-21 June 2007.